RSC Advances

PAPER

View Article Online
View Journal | View Issue

Cite this: *RSC Adv.*, 2023, **13**, 32110

Facile one pot synthesis of 2-substituted benzimidazole derivatives under mild conditions by using engineered MgO@DFNS as heterogeneous catalyst

Suman Kusuma,[ab] Dipak B. Bawiskar,[a] Chob Singh,[a] Pratheep Panneerselvam,[a] Pradipta Sinha,[b] Akshaya K. Samal[a] and Arvind H. Jadhav[*a]

Benzimidazole derivatives are considered as important heterocyclic motifs that show a wide range of pharmaceutical applications. In view of their wide-ranging bioactivities, it is imperative to direct research on the sustainable catalytic synthesis of benzimidazole. Therefore, herein, we report a novel approach for the synthesis of benzimidazole and its derivatives with engineered MgO supported on dendritic fibrous nano silica (MgO@DFNS) as a sustainable heterogeneous catalyst. The catalyst MgO@DFNS was thoroughly characterized to understand its physio-chemical properties using XRD, FE-SEM, XPS, FT-IR, zeta potential, HR-TEM, TGA, TPR and TPD. The obtained results suggested that the catalyst MgO@DFNS prepared well and have the desired characteristics in it. After the successful characterisation of the prepared catalyst MgO@DFNS, it was applied in the synthesis of benzimidazole derivatives *via* condensation of *o*-phenylenediamine, and various aromatic and aliphatic aldehydes under ambient temperature. The catalyst produced a clean reaction profile with excellent yields in a shorter time under the umbrella of green chemistry. The effect of reaction parameters such as the effect of time, catalyst dosage, loading of MgO, effect of solvents and effect of different homo and heterogeneous catalyst were also tested. Furthermore, to understand the scope of the catalyst different substituted diamines and substituted aldehydes were reacted and obtained desired products in good to efficient yield. In addition, a recyclability study was also conducted and it was observed that the catalyst could be recycled for up to six cycles without noticeable changes in the morphology and activity. We believe that the present methodology gave several advantages such as an eco-friendly method, easy work-up, good selectivity, high yields and quick recovery of catalyst. MgO@DFNS is highly stable for several cycles without significant loss of its activity, which possibly demonstrates its applicability at the industrial scale.

Received 23rd August 2023
Accepted 22nd October 2023

DOI: 10.1039/d3ra05761e

rsc.li/rsc-advances

1. Introduction

Benzimidazole is a hetero bicyclic aromatic compound which is a fusion of benzene and imidazole rings.[1] Benzimidazole and its derivatives have many applications in therapeutic areas such as antimicrobial agents,[2] antiviral agents against several viruses such as HIV,[3] influenza,[4] antitumor,[5] anti-inflammatory[6] as well as antiprotozoal agents.[7] Benzimidazole moieties play a crucial role in the treatment of ulcers, as an antihelminth and anti-histamine agent. The benzimidazole ring is an essential pharmacophore in current drug discovery. Synthesis of novel benzimidazole and its derivatives are the main focus of medicinal research. Recently, researchers are focusing on substituted benzimidazole, which shows easy interactions with the biopolymers, and possesses potential activity with lower toxicities in the chemotherapeutic approach in humans (Haugwitz *et al.*, 1982). Benzimidazole and its derivatives are important intermediates because of their pharmacology properties. Moreover, various synthetic methodologies have been reported from different reactants and reaction conditions such as the reaction between *o*-phenylenediamine and carboxylic acid,[8,9] condensation between *o*-phenylenediamine and aldehydes catalyzed by metal triflates such as $Sc(OTf)_3$,[10] H_2O_2/HCl,[11] different oxidizing agents[12–14] and lanthanides such as Lewis acid catalysts for the synthesis of benzimidazole derivatives.[15]

Nanomaterials have emerged as superior alternatives to conventional materials for various organic transformations. Their advanced applicability in heterogeneous catalysis and as catalyst supports is attributed to their higher surface area, unique textural and structural properties.[16] Supported metal

[a]*Centre for Nano and Material Sciences, JAIN University, Global Campus, Bengaluru 562112, Karnataka, India. E-mail: j.arvind@jainuniversity.ac.in; jadhav.ah@gmail.com*

[b]*Aragen Life Science Pvt. Ltd., Plot No. 284-A (Part), Bommasandra, Bengaluru 562106, India*

nanoparticles have garnered more attention than unsupported ones due to their large surface and volume ratio, intramolecular bonding, surface interaction, and interaction between metal–support.[16]

In addition, SiO_2 as a solid support[17] and its provides additional characteristics in the reactions such as high surface area, high active sites uniform distribution, catalyst strength and easy of recyclability. For the particular silica supported polyphosphoric acid has been used as a catalyst under MW irradiation[18] many more catalytic process have been developed with the SiO_2 supported system and showed efficient to good yield.[17,18] However, many of these methodologies have some disadvantages such as low yields, prolonged reaction time, high temperature, the excess requirement of catalysts, harsh reaction conditions, difficulty in extraction of product, difficulty in recovery of catalyst, formation of byproduct *etc.* Therefore, it is necessary to adopt a simpler and more efficient protocol for the synthesis of benzimidazole derivatives.

Our research group has previously successfully reported the multiple heterogeneous nanocatalysts for the synthesis of various organic scaffolds such as benzimidazole,[19,20] Sustainable fixation of CO_2 into epoxides to form cyclic carbonates,[21] and chemical conversion of fructose into 5-hydroxymethylfurfural (HMF).[22] Herein we introduce a novel engineered MgO@DFNS catalyst for the one pot synthesis of 2-substituted benzimidazole derivatives under greener conditions. The catalyst MgO@DFNS has thoroughly characterized to understand its physio-chemical properties using XRD, FE-SEM, XPS, FT-IR, zeta potential, HR-TEM, TGA, TPR and TPD. The obtained material has found to be steady under the employed reaction conditions and easily recovered and recycled up to six times without any considerable loss in the yield.

2. Materials and methods

2.1. Materials

Cetyl trimethyl ammonium bromide (CTAB, purity 99%), tetraethylorthosilicate (TEOS, 99%) were purchased from Sigma-Aldrich, magnesium oxide (MgO, purity 99%), $Mg(NO_3)_2 \cdot 6H_2O$, pentanol (99%), urea were procured from Sigma-Aldrich, India. Acetonitrile (99%), methanol (99%), tetrahydrofuran (99%), *n*-hexane (99%), ethanol (99%), diethyl ether (99%), cyclohexane (99%), and chloroform (purity 99%) solvents were supplied by Sd Fine Chem. Limited. All substituted *o*-phenylenediamines (OPDA) and different substituted aldehydes were obtained from Sigma-Aldrich, India (purity 99%).

2.2. Synthesis of MgO@DFNS catalyst

2.2.1 Preparation of dendritic fibrous nano silica (DFNS). DFNS were prepared by following the reported procedure.[23] Precisely, 2 g CTAB was taken in a 250 mL 2-neck round bottom (RB) flask. Then, 1.2 g of urea and 20 mL of DI water were added to the RB and stirred (1300 rpm) for 3 h. To this, a freshly prepared solution of TEOS (4 g), cyclohexane (60 mL), and pentanol (3 mL) was added dropwise and then the mixture was refluxed for 24 h. The reaction mixture was cooled to room temperature, filtered and washed with excess water followed by ethanol to obtain DFNS. The collected DFNS was dried in a vacuum oven at 60 °C for 24 h. Finally, the material was calcinated at 550 °C for 6 h to remove CTAB as a templating agent and other organic components to obtain pure DFNS.

2.2.2 Preparation of MgO@DFNS. MgO@DFNS catalysts were prepared by the following procedure, the freshly prepared pristine DFNS (0.126 g) was added to $Mg(NO_3)_2 \cdot 6H_2O$ (0.089 g) in 60 mL of DI water under a stirring condition once it form homogeneous solution then heated to 90 °C for 1 h. The reaction mixture was cooled to room temperature and then the solution mixture was washed with ethanol and water several times to remove the unreacted materials. The final residue was collected in a Petri dish and then dried in a vacuum oven at 70 °C for 16 h. The collected final powder was then calcinated at 450 °C for 4 h in a normal atmosphere to remove other organic components present in the preparation producer to obtain pure MgO@DFNS catalyst.[24,25]

2.3. Characterization techniques

The physicochemical features of the synthesized catalyst were studied by using several advanced characterization techniques. The presence of functional groups in the prepared samples was analyzed by using FT-IR spectroscopy. PerkinElmer FT-IR spectrophotometer (Spectrum Two) instrument was used to record FT-IR spectra by using KBr (IR grade) pellet method. The information on crystalline nature and phase development were obtained from their respective powder X-ray diffraction (XRD) patterns recorded on an X-ray diffractometer (XRD; Rigaku Japan) with Cu Kα radiation source ($\lambda = 1.5406$ Å). The spectra were recorded between the 10 and 80° range and a scan rate of $2° \text{ min}^{-1}$.

The TGA analysis of prepared catalysts was performed to understand their decomposition process. The thermal analysis was performed from room temperature to 800 °C at a heating rate of 10 °C min^{-1} under N_2 flow on a Scinco TGA N-100 instrument. Field emission scanning electron microscopy (FE-SEM), was used to gain morphological and topographical information. Prior to the analysis, the samples were evenly coated on the carbon tape placed on an aluminium metal stub. The sample on the stub was then sputtered by gold nanoparticles for 120 s and the analysis was executed by using FE-SEM (JEOL Model-JSM7). X-ray photoelectron spectroscopy (XPS) analysis was employed to understand elemental composition as well as the electronic state of the elements in the samples. The analysis were performed on an X-ray photoelectron spectrometer (PerkinElmer PHI1257) at 4×10^{-10} torr pressure with Al Kα X-ray as the excitation source (1486.7 eV).

Brunauer–Emmett–Teller (BET) and Barrett–Joyner–Halenda (BJH) methods were used, respectively to evaluate the specific surface area and pore size distribution of the materials. The analysis was performed on the Belsorp MAX instrument (BEL Japan) at the temperature of liquid nitrogen. The materials were degassed at 100 °C for 2 h in a high vacuum before the analysis. Additionally, the acidic sites in the samples were quantified by using NH_3-TPD analysis using pure ammonia gas (99.999% purity). The TPD instrument was designed by handmade set-up,

the quartz tube (length: 300 mm, inner diameter: 6 mm) was connected to a six-port valve with thermal conductivity detector (M/s. Mayura Analytical Pvt. Ltd., India).

^{1}H-NMR spectra were recorded on Varian Gemini (400 MHz) spectrometer using DMSO-d_6 as a solvent and tetramethylsilane (TMS) as an internal standard. ^{13}C-NMR spectra were also recorded on 100 MHz in the same solvent. The reactions were monitored by Thin Layer Chromatography (TLC) on silica gel plates using pet ether and ethyl acetate as a solvent system. The melting points of the respective samples were recorded using the Sigma Scientific instrument.

2.4. General procedure for the synthesis of benzimidazole derivatives over synthesized MgO@DFNS catalyst

A mixture of *o*-phenylenediamine (OPD) (1 mmol) and aldehyde (1.1 mmol) in ethanol was placed in a two-neck round bottom flask and the required amount of 10 wt% MgO@DFNS catalyst was added to the reaction mixture at room temperature (RT) and stirred for 3 h. After completion of the reaction (monitored by TLC), the reaction mixture was filtered through the filter paper to separate the catalyst. The filtrate was evaporated under reduced pressure to afford crude product. The obtained crude product was purified by silica gel (100–200 mesh) column chromatography using ethyl acetate/pet ether as an eluent in a 20 : 80 ratio to obtain pure compounds. The obtained compounds were characterized by ^{1}H NMR, ^{13}C-NMR and mass spectroscopy and also compared with the literature values. The filtered catalyst was dried overnight at 80 °C and reused for the further cycles.[21,26]

2.4.1 2-Phenyl-1*H*-benzo[*d*]imidazole (1): off-white solid: mp 292–296 °C. ^{1}H NMR (400 MHz, DMSO-d_6): δ 12.92 (bs, 1H), 8.19 (d, J = 7.2 Hz, 1H), 7.60–7.48 (m, 5H), 7.22–7.20 (m, 2H), 3.10 (bs, 1H), 2.62–2.57 (m, 2H), 2.21 (q, J = 12.8 Hz, 2H), 1.68–1.57 (m, 2H), 1.26 (S, 6H), 0.963 (t, J = 7.6 Hz, 3H). ^{13}C NMR (100 MHz, DMSO-d_6): δ 151.1, 130.1, 129.7, 128.9, 126.4, 122.0, 118.8, 111.3: LCMS: m/z 195.09 (M + H)$^+$.

2.4.2 2-(3-Methoxyphenyl)-1*H*-benzo[*d*]imidazole (2): brown solid: mp 205–209 °C. ^{1}H NMR (400 MHz, DMSO-d_6): δ 12.88 (bs, 1H), 7.75 (d, J = 7.2 Hz, 2H), 7.66 (d, J = 7.2 Hz, 1H), 7.53 (d, J = 8.0 Hz, 1H), 7.21 (m, 2H), 7.06 (d, J = 8.0 Hz, 1H), δ 3.86 (s, 1H); ^{13}C NMR (100 MHz, DMSO-d_6): δ 160.1, 151.5, 131.9, 130.5, 122.8, 119.2, 116.3, 11.8, 55.7: LCMS: m/z 225.26 (M + H)$^+$.

2.4.3 2-(3-Chlorophenyl)-1*H*-benzo[*d*]imidazole (3): brown solid: mp 233–237 °C. ^{1}H NMR (400 MHz, DMSO-d_6): δ 13.02 (bs, 1H), 8.23 (s, 1H), 8.15 (d, J = 6.8 Hz, 1H), 7.67–7.57 (m, 4H), 7.24 (s, 2H): ^{13}C NMR (100 MHz, DMSO-d_6): δ 150.1, 144.0, 135.4, 134.2, 132.6, 131.4, 130.0, 126.4, 125.4, 123.4, 122.4, 119.5, 111.9: LCMS: m/z 229.02 (M + H)$^+$.

2.4.4 2-Cyclohexyl-1*H*-benzo[*d*]imidazole (4): off-white solid: mp 281–285 °C. ^{1}H NMR (400 MHz, DMSO-d_6): δ 12.05 (bs, 1H), 7.50 (d, J = 6.8 Hz, 1H), 7.38 (d, J = 8.0 Hz, 1H), 7.12–7.06 (m, 2H), 2.85 (m, 1H), 2.01 (m, 2H), 1.81–1.55 (m, 5H), 1.43–1.27 (m, 3H): ^{13}C NMR (100 MHz, DMSO-d_6): δ 158.8, 143.0, 134.1, 121.2, 120.9, 118.1, 110.6, 110.4, 37.6, 31.2, 25.5: LCMS: m/z 201.10 (M + H)$^+$.

2.4.5 2-Phenethyl-1*H*-benzo[*d*]imidazole (5): off-white solid: mp 188–192 °C. ^{1}H NMR (400 MHz, DMSO-d_6): δ 12.23 (bs, 1H), 7.51–7.40 (m, 2H), 7.29–7.24 (m, 4H), 7.19–7.15 (m, 1H), 7.11–7.10 (m, 2H), 3.11 (S, 4H): ^{13}C NMR (100 MHz, DMSO-d_6): δ 154.2, 143.2, 141.0, 134.2, 128.3, 128.2, 125.9, 121.3, 120.7, 118.0, 110.6, 33.2, 30.3: LCMS: m/z 223.10 (M + H)$^+$.

2.4.6 2-(Naphthalen-2-yl)-1*H*-benzo[*d*]imidazole (6): pale yellow solid: mp 276–280 °C. ^{1}H NMR (400 MHz, DMSO-d_6): δ 12.94 (bs, 1H), 9.12 (d, J = 8.0 Hz, 1H), 8.11–8.02 (m, 3H), 7.80–7.58 (m, 5H), 7.27 (t, J = 6.8 Hz, 2H): ^{13}C NMR (100 MHz, DMSO-d_6): δ 151.3, 143.8, 134.4, 133.5, 130.4, 130.1, 128.3, 127.8, 127.4, 127.0, 126.3, 125.2, 122.6, 121.5, 119.0, 111.3: LCMS: m/z 245.10 (M + H)$^+$.

2.4.7 2-Propyl-1*H*-benzo[*d*]imidazole (7): off-white solid: mp 154–158 °C. ^{1}H NMR (400 MHz, DMSO-d_6): δ 12.16 (bs, 1H), 7.50–7.40 (m, 2H), 7.10–7.09 (m, 2H), 2.77 (t, J = 7.6 Hz, 2H), 1.83–1.74 (m, 2H), 0.94 (t, J = 7.6 Hz, 3H): ^{13}C NMR (100 MHz, DMSO-d_6): δ 154.9, 143.3, 134.2, 121.2, 120.6, 118.0, 110.6, 30.4, 20.9, 13.6: LCMS: m/z 161.20 (M + H)$^+$.

2.4.8 2-(Furan-2-yl)-1*H*-benzo[*d*]imidazole (8): light orange solid. ^{1}H NMR (400 MHz, DMSO-d_6): δ 12.90 (bs, 1H), 7.94 (S, 1H), 7.62 (d, J = 7.2 Hz, 1H), 7.49 (d, J = 7.2 Hz, 1H) 7.27–7.16 (m, 3H), 6.73–6.72 (m, 2H): ^{13}C NMR (100 MHz, DMSO-d_6): δ 145.5, 144.5, 143.6, 134.2, 122.5, 121.7, 118.7, 112.2, 111.3, 110.4: LCMS: m/z 185.01 (M + H)$^+$.

2.4.9 2-(4-Fluorophenyl)-1*H*-benzo[*d*]imidazole (9): light yellow solid: mp 252–256 °C. ^{1}H NMR (400 MHz, DMSO-d_6): δ 12.92 (bs, 1H), 8.25–8.21 (m, 2H), 7.66 (d, J = 6.4 Hz, 1H), 7.54 (d, J = 6.4 Hz, 1H), 7.43–7.38 (m, 2H), 7.21 (bs, 2H): ^{13}C NMR (100 MHz, DMSO-d_6): δ 164.2, 161.8, 150.3, 143.7, 134.9, 128.7, 128.6, 126.8, 126.7, 122.5, 121.6, 118.8, 116.0, 115.8, 111.2: LCMS: m/z 213.09 (M + H)$^+$.

2.4.10 2-(4-(Trifluoromethyl)phenyl)-1*H*-benzo[*d*]imidazole (10): off-white solid: mp 273–277 °C. ^{1}H NMR (400 MHz, DMSO-d_6): δ 13.18 (bs, 1H), 8.40 (d, J = 8.0 Hz, 2H), 7.94 (d, J = 8.0 Hz, 2H), 7.71–7.59 (m, 2H), 7.26 (s, 2H): ^{13}C NMR (100 MHz, DMSO-d_6): δ 149.6, 143.6, 135.0, 133.9, 129.5 (q, J = 31.5 Hz); LCMS: m/z 263.04 (M + H)$^+$.

2.4.11 Methyl 4-(1*H*-benzo[*d*]imidazol-2-yl)benzoate (11): off white solid: mp 230–234 °C. ^{1}H NMR (400 MHz, DMSO-d_6): δ 13.14 (bs, 1H), 8.32 (d, J = 8.4 Hz, 2H), 8.13 (d, J = 8.4 Hz, 2H), 7.70–7.58 (m, 2H), 7.25 (s, 2H), 3.90 (s, 3H): ^{13}C NMR (100 MHz, DMSO-d_6): δ 165.7, 149.9, 143.7, 135.0, 134.3, 130.2, 129.7, 126.5, 123.1, 122.0, 119.1, 111.5, 52.2: LCMS: m/z 253.01 (M + H)$^+$.

2.4.12 2-(*p*-Tolyl)-1*H*-benzo[*d*]imidazole (12): brown solid: mp 281–284 °C. ^{1}H NMR (400 MHz, DMSO-d_6): δ 12.82 (bs, 1H), 8.07 (d, J = 7.6 Hz, 2H), 7.63–7.52 (m, 2H), 7.36 (d, J = 8.4 Hz, 2H), 7.19 (s, 2H), 2.38 (s, 3H): ^{13}C NMR (100 MHz, DMSO-d_6): δ 151.3, 143.7, 139.5, 134.9, 129.4, 127.4, 126.3, 122.2, 121.5, 118.6, 111.1, 20.9: LCMS: m/z 209.10 (M + H)$^+$.

2.4.13 2-Phenyl-1*H*-naphtho[2,3-*d*]imidazole (13): brown solid: mp 193–197 °C. ^{1}H NMR (400 MHz, DMSO-d_6): δ 12.95 (bs, 1H), 8.30 (d, J = 1.2 Hz, 2H), 8.21 (s, 1H), 8.03–8.01 (m, 3H), 7.57–7.38 (m, 5H), 7.38 (bs, 2H): ^{13}C NMR (100 MHz, DMSO-d_6): δ 155.3, 144.3, 135.7, 130.6, 130.2, 129.7, 129.0, 128.0, 127.3, 127.0, 123.7, 123.0, 115.2, 106.5: LCMS: m/z 245.20 (M + H)$^+$.

2.4.14 2-(2-Bromophenyl)-1*H*-naphtho[2,3-*d*]imidazole (14): brown solid. ^{1}H NMR (400 MHz, DMSO-d_6): δ 12.87 (bs, 1H), 8.15 (bs, 2H), 8.03 (bs, 2H), 7.87–7.85 (m, 2H), 7.61–7.50 (m, 2H), 7.40–7.39 (m, 2H): ^{13}C NMR (100 MHz, DMSO-d_6): δ 154.7, 133.4, 132.2, 132.1, 131.8, 129.9, 127.8, 127.7, 123.4, 121.5: LCMS: m/z 323.24 $(M + H)^+$.

2.4.15 2-(3-Chlorophenyl)-1*H*-naphtho[2,3-*d*]imidazole (15): yellow solid: mp 178–182 °C. ^{1}H NMR (400 MHz, DMSO-d_6): δ 13.07 (bs, 1H), 8.34 (d, J = 1.2 Hz, 1H), 8.33–8.24 (m, 2H), 8.03–8.01 (m, 3H), 7.67–7.62 (m, 2H), 7.42–7.36 (m, 2H): ^{13}C NMR (100 MHz, DMSO-d_6): δ 153.8, 144.0, 135.6, 133.8, 131.7, 131.0, 130.4, 130.3, 129.8, 128.1, 127.3, 126.6, 125.6, 123.9, 123.1, 115.5, 106.7: LCMS: m/z 279.22 $(M + H)^+$.

3. Results and discussion

3.1. MgO@DFNS catalyst characterization

3.1.1 FT-IR analysis. The prepared 10 wt% MgO@DFNS catalyst and pristine DFNS were characterized by FT-IR spectroscopic technique. The FT-IR spectra of both pristine DFNS and 10 wt% MgO@DFNS catalyst are presented in Fig. 1. It shows three broad absorption regions in the range of 3200–3600, 800–1200, and 450–600. The broad peak located at 3435 cm^{-1} can be attributed to free-standing O–H stretching vibration and hydrogen bonding related to the possible presence of a large number of Si–OH groups.[27] The broad absorption peak located at 1631 cm^{-1} is associated with O–H bending vibration. The characteristic broad peak at 1092 cm^{-1} is due to the asymmetric stretching vibration and the peak at 750 cm^{-1} is due to the symmetric stretching vibration of Si–O–Si.[28] The band at 468 cm^{-1} corresponds to the Si–O–Si bending vibration. The FT-IR spectrum of the MgO@DFNS catalyst suggested the presence of Mg–O–Si and Mg–O stretching vibration bands at 942 cm^{-1} and 468 cm^{-1}, respectively. It provides strong evidence for the formation of MgO@DFNS that the shoulder peak at 942 cm^{-1} is corresponding to Mg–O–Si stretching vibration. The appearance of Si–O–Si peaks at 1092, 750, and 468 cm^{-1} and the increase in the intensity of O–H peaks at 3435 and 1438 cm^{-1} after added silica with MgO suggest strong indication for silica incorporation into the surface of MgO and the development of Si–O–Mg links.[29,30] The FT-IR spectra of DFNS and MgO@DFNS demonstrated an almost similar pattern and suggests the successful formation of MgO@DFNS catalyst.

3.1.2 XRD analysis. The crystalline nature and phase of the final catalyst were analysed along with pristine MgO and pristine DFNS with the assistance of XRD analysis. The XRD patterns of 10 wt% MgO@DFNS and pristine DFNS are shown in Fig. 2. The pristine DFNS exhibited a broad peak and it is observed in the range of 20–30°. The broad peak observed is due to the presence of amorphous silica nanoparticles (NPs) with dendrimeric fibre structure.[31] The as-prepared MgO shows $Mg(OH)_2$ structure with two prominent diffraction peaks precisely at 38.2° and 57.8° corresponding to the (101) and (103) planes, respectively along with 3 minor peaks and also matched with the JCPDS no. 03-0998.[24] However XRD pattern of 10 wt% MgO@DFNS reveals the absence of sharp intense peaks and shows only a broad peak in the range of 20–30° due to the presence of a high percentage of amorphous silica present in the MgO@DFNS system. There is no identification of MgO as well as $Mg(OH)_2$ presence in the 10 wt% MgO@DFNS. This is may be the less percentage of MgO in the DFNS system. To confirm the formation of MgO@DFNS we have increased the wt% to 50% and its XRD pattern reveals the existence of MgO@DFNS by the presence of the peaks precisely at 42.8° and 62.6° corresponding to the (200) and (220) planes, respectively. This result is also well matched with the JCPDS no. 45-0946. The XRD peak for 10 wt% MgO@DFNS sample exhibited a broad peak compared to pristine DFNS which indicates that MgO particles are adsorbed by amorphous DFNS. The presence of MgO@DFNS is also a good argument with the FTIR result and is further confirmed with XPS analysis.

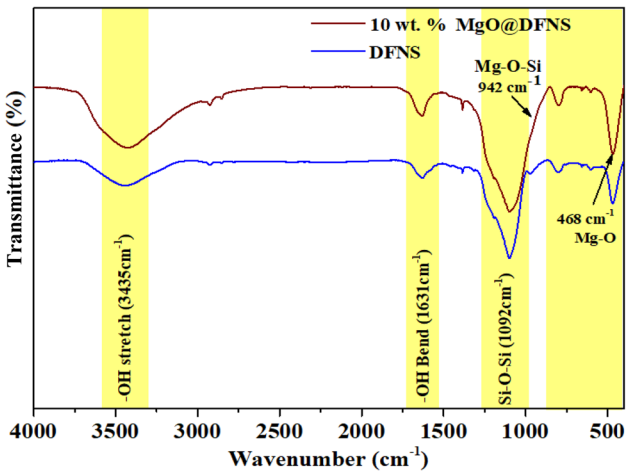

Fig. 1 FT-IR spectra of pure DFNS and 10 wt% MgO@DFNS catalyst.

3.1.3 TGA analysis. TGA analysis of the pristine DFNS and 10 wt% MgO@DFNS was performed from ambient temperature to 800 °C and obtained curves are shown in Fig. 3. The TGA curve of pristine DFNS shows a weight loss of 4.5% of its initial weight occurs at ~below 100 °C. This weight loss is due to the elimination of both physisorbed and chemisorbed water,

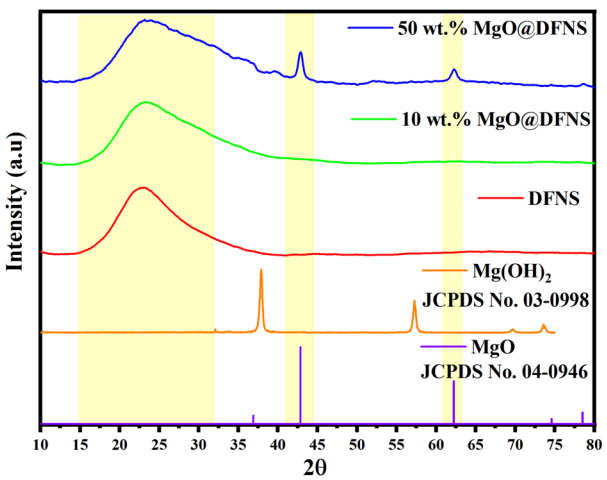

Fig. 2 XRD pattern of MgO@DFNS catalyst.

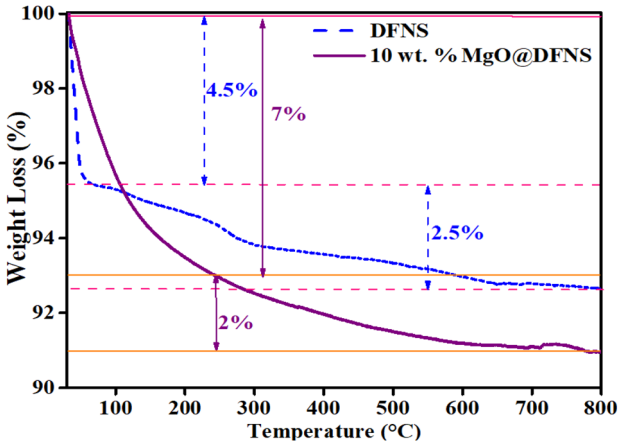

Fig. 3 TGA analysis of pure DFNS and 10 wt% MgO@DFNS catalyst.

alcohol and solvents over the silica surface.[32] The second weight loss of ~2.5% took place between 100 and 600 °C this wide range centred at ~370 °C. This weight loss arises due to dehydroxylation and loss of water or alcohol from silica precursors.[30] The final weight loss of 6% from its initial weight is obtained for pristine DFNS. The TGA curve of 10 wt% MgO@DFNS displayed only one major weight loss in the temperature range of ~RT-300 °C is due to the elimination of both physisorbed and chemisorbed water, alcohol and solvents presented in the sample. After 300 °C the weight is very less and becomes constant with the increasing temperature due to the crystalline nature of MgO. The overall final weight loss is 9% from its initial weight and the increased weight loss over the pristine DFNS sample. The difference between the total loss of the two materials (3%) is probably due to the addition of MgO and it reveals excellent grafting of MgO over DFNS and successful formation of MgO@DFNS.

3.1.4 FE-SEM and EDAX analysis. To know the morphology, shape and size of the prepared catalyst, we performed FE-SEM analysis of pristine DFNS as well as 10 wt% MgO@DFNS catalyst and obtained images are shown in Fig. 4. The FE-SEM images of DFNS displayed monodispersed spherical morphology without any complex structure.[24] The morphology was found to be retained in the final catalyst even after deposition of MgO indicating crystalline and stable morphology.

Further, EDAX analysis (Fig. 5) of DFNS and 10 wt% MgO@DFNS suggested the presence of all the expected elements in the prepared catalyst in the stoichiometric amount. Additionally, MgO particles were uniformly distributed over the DFNS surface as could be observed from mapping analysis.

3.1.5 H_2 temperature-programmed reduction (H_2-TPR) analysis. The H_2-TPR profile of the pristine DFNS and 10 wt% MgO@DFNS catalyst are shown in Fig. 6. We have observed only one reduction peak for 10 wt% MgO@DFNS catalyst only and this reduction peaks could be attributed to the release of H_2 adsorbed on the catalyst surface by its excellent hydrogen absorbent property.[33] The H_2-TPR profile of pristine DFNS showed a flat line with the absence of any reduction bands; it clearly states that DFNS does not have reducible as well as there are no other reduction sites. At the same time, the H_2-TPR profile of prepared 10 wt% MgO@DFNS catalyst showed one intense reduction band centred at 656 °C ascribed to a reduction of Mg^{2+} to Mg^0. It is known that the reduction reaction between MgO and H_2 can be represented with the following equation, $MgO + H_2 \rightarrow Mg^{(0)} + H_2O_{(g)}$.[34]

3.1.6 NH_3-TPD analysis. The acidic sites in the catalyst are essentially important in the synthesis of benzimidazole derivatives from their raw materials.[35] Therefore, NH_3-TPD analysis was performed to quantify the amount and the strength of acidic sites present in the prepared catalyst as represented in Fig. 7. From the TPD profile of the final catalyst, we observed prominent peaks in all three regions. A major peak was observed in the temperature range 100–300 °C corresponding to the presence of weak acidic sites. Moreover, literature also suggested that NH_3 interacting with Lewis acidic sites desorbs

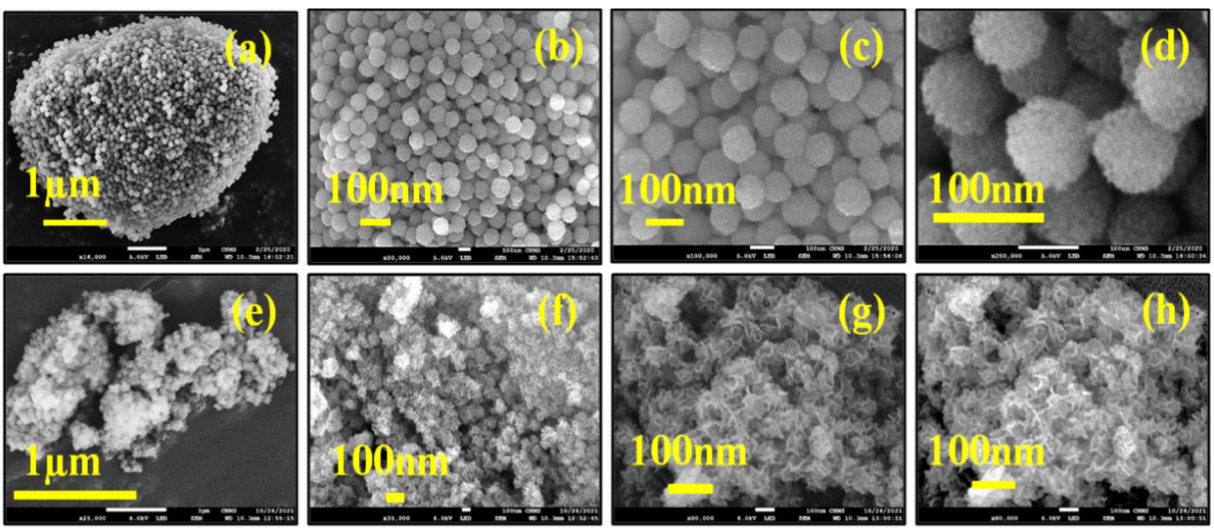

Fig. 4 FE-SEM analysis of SEM DFNS (a–d) and 10 wt% MgO@DFNS (e–h).

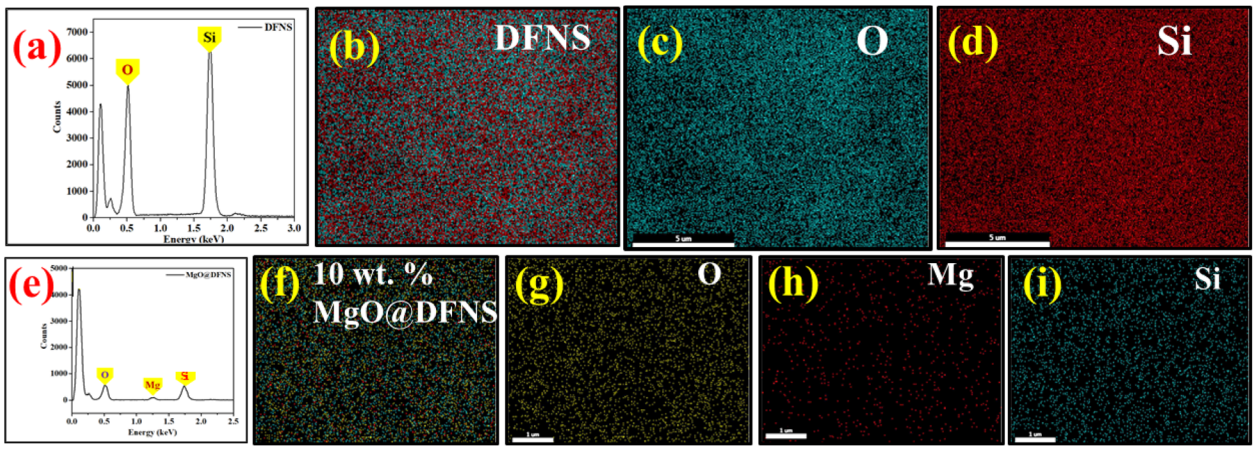

Fig. 5 EDX analysis of DFNS (a–d) and 10 wt% MgO@DFNS (e–i).

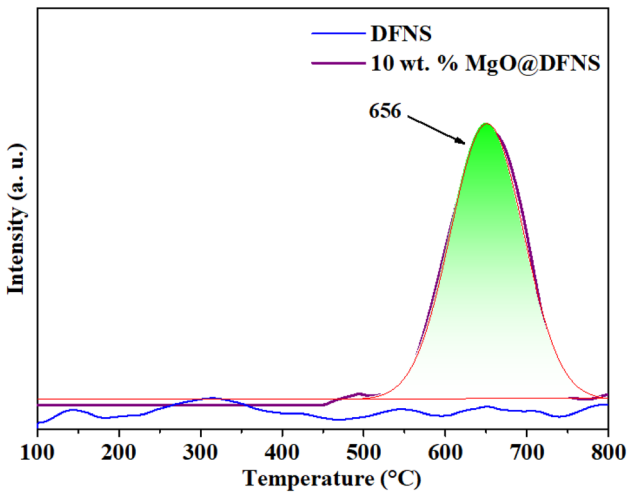

Fig. 6 H_2-TPR analysis of DFNS and 10 wt% MgO@DFNS.

in this temperature region.[33] The peaks in the temperature range of 300–500 °C represented moderate acidic sites and very low intense peaks were observed in the temperature range of 500–700 °C as a result of the presence of strong acidic sites in this region. The amount of total acidic sites in the 10 wt% MgO@DFNS catalyst was calculated from TPD data was 0.324 mmol g^{-1} which could be sufficient to promote conversion of benzimidazole derivatives from corresponding aldehyde and diamines. However, the TPD data of DFNS did not show any definite peaks in all areas signifying the presence of less acidic sites which was calculated 0.0231 mmol g^{-1}.[36]

3.1.7 XPS analysis. The XPS analysis of pristine DFNS and MgO@DFNS was performed and is shown in Fig. 8. The survey scan spectra of pristine DFNS indicated that the elements present in the sample such as O, C, and Si. The corresponding high-resolution XPS (HR-XPS) spectra of Si 2p and O 1s are presented in Fig. 8(b) and (c). A trace of C element presence can be due to the unreacted product in the sample. The HR-XPS of Si 2p is shown in Fig. 8(b), the deconvolution of it exhibited two peaks and it is suggested by the presence of Si–O–Si at 103.6 eV and chemisorbed species at 105.1 eV, respectively.[37] The absorbed Si 2p signal at 103.6 eV reveals the existence of SiO_2 (Si^{4+}).[38] De-convolution of O 1s resulted in two peaks at 533.24 eV and 532.61 eV corresponding to Si–O–Si bonds and Si–O bands present in DFNS NPs.[36] On the other hand, the XPS survey scan spectrum of MgO@DFNS shown in Fig. 8(a) Mg 1s along with Si 2p peak and reveals the successful formation of MgO@DFNS sample also a good argument with the FTIR result. We observed a slight shift in binding energy values in Si 2p and O 1s. This observation could be attributed to the presence of MgO particles strongly bonded with DFNS. As shown in Fig. 8(d), a major peak observed at 1304.18 eV and a minor peak at 1303.2 eV could be Mg–O and Mg–OH bonds, respectively and the majority of Mg is in the form of MgO with traces amount of $Mg(OH)_2$.[39] Fig. 8(e) shows the Si 2p peaks deconvoluted with 2 peaks located at 105.14 due to the Si–O–Mg interaction along with the Si–O–Si interaction peak located at 102.78 representing the Si^{4+} state. De-convolution of O 1s resulted in a small peak at 529.6 eV corresponds to the presence of the Mg–OH group suggesting the presence of oxide or hydroxyl groups[40] which is

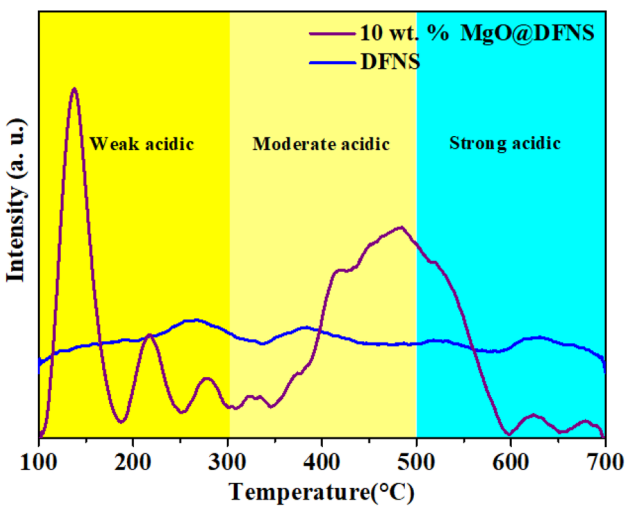

Fig. 7 NH_3-TPD analysis of DFNS and 10 wt% MgO@DFNS.

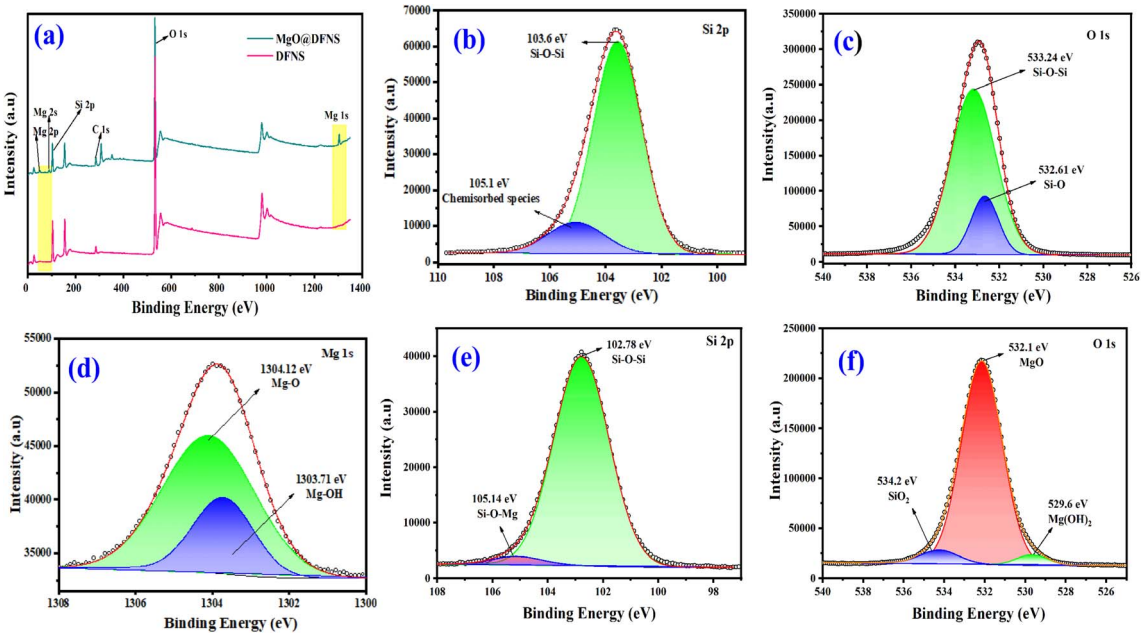

Fig. 8 (a) Survey spectrum of pristine DFNS and MgO@DFNS, deconvoluted spectra of (b) Si 2p, (c) O 1s and (d) deconvoluted spectra of Mg 1s (e) Si 2p, (f) O 1s.

also supported by FT-IR analysis. The presence of the peak at 532.1 eV is due to the formation of MgO as well as the peak located at 534.2 is due to the presence of SiO_2.[25,39,41]

3.1.8 N_2-adsorption analysis. To study the surface area and pore diameter of prepared pristine DFNS and 10 wt% MgO@DFNS catalyst, we performed N_2 adsorption and the

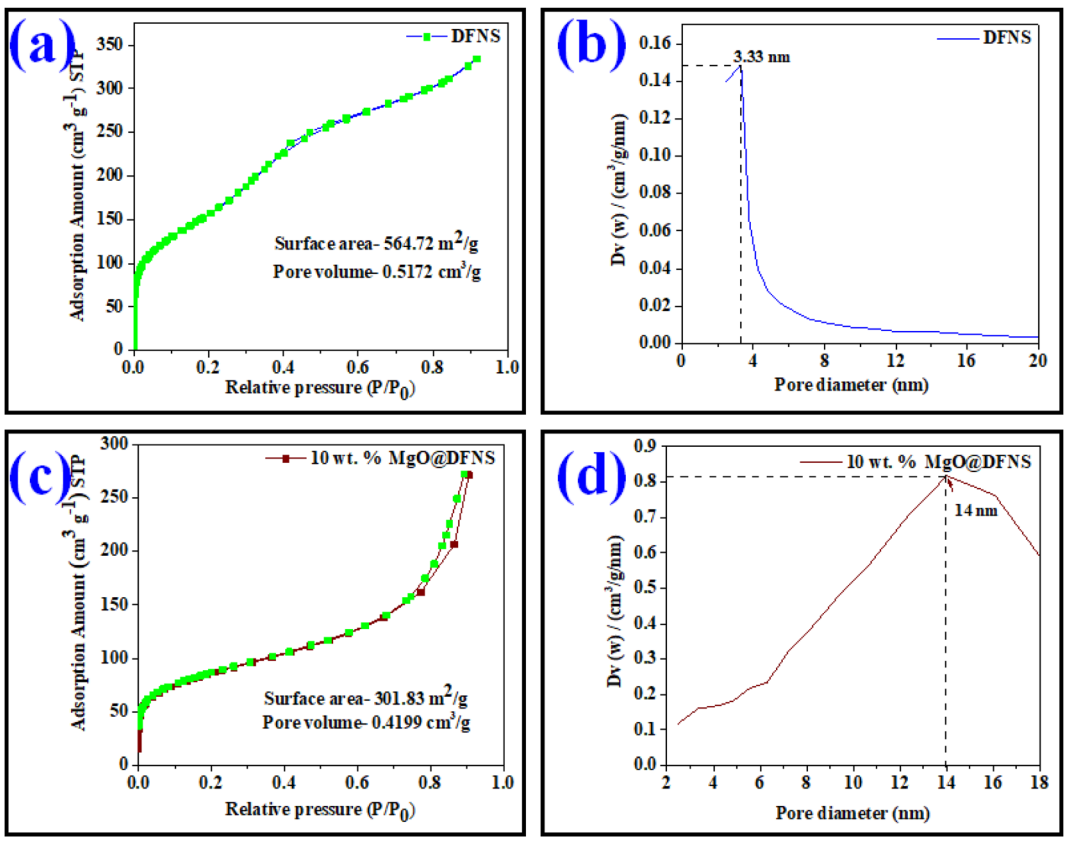

Fig. 9 N_2-adsorption of DFNS and 10 wt% MgO@DFNS.

Table 1 N_2 adsorption–desorption isotherms results of the samples

Entry	Sample	Specific surface area ($m^2\ g^{-1}$)	Mean pore diameter (nm)	Mean pore volume ($cm^3\ g^{-1}$)
1	DFNS	564.72	3.33	0.5172
2	10 wt% MgO@DFNS	301.83	14.0	0.4199

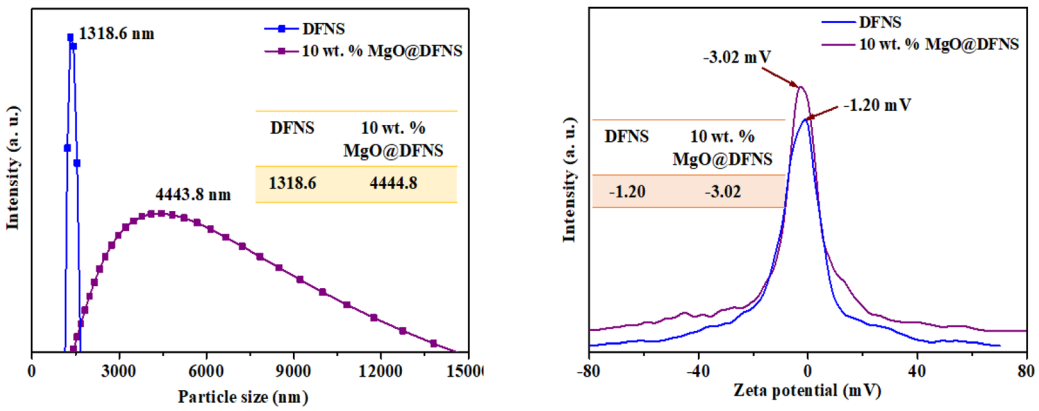

Fig. 10 DLS and zeta potential analysis of DFNS and 10 wt% MgO@DFNS.

results are represented in Fig. 9 and Table 1. As can be observed from Fig. 9, DFNS and prepared 10 wt% MgO@DFNS catalyst exhibited type IV isotherm with an H3 hysteresis loop. This phenomenon is exhibited due to the multilayer adsorption and mesoporous structures of the pores present in the system.[42] The surface area of pristine DFNS is 564.72 $m^2\ g^{-1}$ and the 10 wt% MgO@DFNS is 301.83 $m^2\ g^{-1}$. The reduction in the surface area value for 10 wt% MgO@DFNS system is due to the inclusion of MgO nanoparticles over DFNS which leads to the increase in the size as well as cluster formation in the 10 wt% MgO@DFNS. This results in a good argument with FESEM analysis. The pore volume also decreased from 0.5172 $cm^3\ g^{-1}$ to 0.4199 $cm^3\ g^{-1}$ indicating successful inclusion of MgO NPs. The mean pore diameter of DFNS is observed as 3.3 nm whereas 10 wt% MgO@DFNS catalyst exhibited a mean pore diameter of 14.0 nm. From the FESEM analysis pristine DFNS are monodispersed and highly spherical in nature, this result reveals the small pore size presented in the system. At the same time 10 wt% MgO@DFNS shows the dendrimeric structure and with agglomerated cluster formation presented, it creates a bigger pore size compared to the pristine DFNS. The results obtained from the BET and BJH analysis are represented in Table 1.

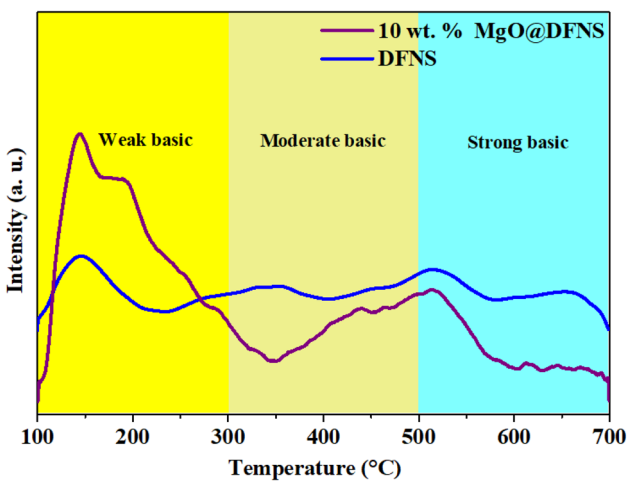

Fig. 11 CO_2-TPD of DFNS and 10 wt% MgO@DFNS.

3.1.9 DLS and zeta potential analysis. DLS and zeta potential analysis was performed to determine the particle size and surface charge of the prepared pristine DFNS and 10 wt% MgO@DFNS catalyst as shown in Fig. 10. The pristine DFNS exhibited the hydrodynamic particle size of 1318 nm, simultaneously 10 wt% MgO@DFNS exhibited 4443 nm nearly. After the successful inclusion of MgO over the DFNS the particle size has increased and confirmed from the FESEM analysis. This resulted in increased hydrodynamic particle size also by the interaction of MgO along with DFNS. The measurement of zeta potential (ZP) depends on the deterioration of NPs caused by electrostatic stress and their surroundings. The hydrogen bond and the electrostatic attraction of DFNS capping MgO resulted in the synthesis of DFNS and MgO@DFNS. ZP was used to assess the stability of synthesized pristine DFNS and MgO@DFNS. The ZP can be used to characterize the surface tension of NPs. The larger value in absolute terms, the higher the electrostatic repulsive force among the two NPs and the reduced surface tension of the NPs. The DFNS surface charge measured as −1.2 mV and 10 wt% MgO@DFNS measured as −3.02 mV. The higher ZP value suggested that highly absorbed molecules on the surface, had highly stable and high catalytic behaviour. These results will help to understand the conversion

Table 2 Optimization of reaction conditions with the MgO@DFNS catalyzed benzimidazole synthesis[a]

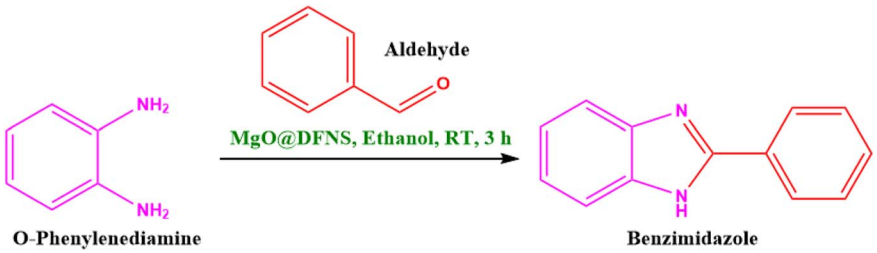

Entry	Reactants	Catalyst dosage (wt%)	Time (h)	[b]Conv./sel. (%)	[b]Yield (%)
1	OPDA, aldehyde	0	4	45/38	32
2	OPDA, aldehyde	0	16	72/54	60
3	OPDA, aldehyde	5.0	3	93/80	85
4	**OPDA, aldehyde**	**10.0**	**3**	**100/90**	**95**
5	OPDA, aldehyde	15.0	3	100/85	92
6	OPDA, aldehyde	20.0	3	100/82	88

[a] Reaction conditions: all reactions proceeded with 1 mmol *o*-phenylenediamine (OPDA), 1.2 mmol aldehyde. [b] Yield refers to an isolated product which characterized by ^{1}H NMR, ^{13}C NMR.

Table 3 Optimization of solvents for the MgO@DFNS catalyzed synthesis of benzimidazole derivatives[a]

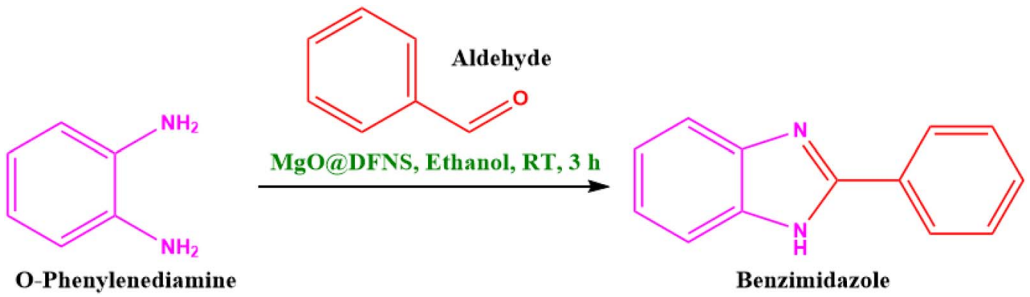

Entry	Solvent (10 mL)	Time (h)	[b]Conv./sel. (%)	[b]Yield (%)
1	Neat	3	100/45	35
2	Acetonitrile	3	97/81	82
3	THF	5	97/84	88
4	1,4-Dioxane	8	85/79	76
5	Chloroform	8	85/72	80
6	*n*-Hexane	6	88/82	72
7	Ethanol	3	100/90	95
8	DMF	3	75/82	60
9	Methanol	4	90/85	85
10	EtOAc	4	80/79	75
11	Ethanol/acetonitrile	4	90/72	70
12	Ethanol/THF	4	74/51	56
13	Ethanol/dioxane	4	83/60	65
14	Ethanol/DMF	4	78/38	41

[a] Reaction conditions: all reactions proceeded with 1 mmol *o*-phenylenediamine (OPDA), and 1.2 mmol aldehyde with MgO@DFNS catalyst (amount of catalyst-5 wt%). [b] Yield refers to an isolated product which characterized by ^{1}H NMR, ^{13}C NMR.

of benzimidazole derivatives and the catalytic behaviour of 10 wt% MgO@DFNS.

3.1.10 CO_2-TPD analysis. The CO_2-TPD analysis was performed to measure the amount and the potency of surface basic sites present in prepared catalysts as represented in Fig. 11. In the CO_2 TPD pattern of the DFNS support, there are three distinct less intense CO_2 desorption peaks (at 150 °C, 350 °C & 510 °C) at <600 °C, which have been assigned as various types of basic sites based on their strength, *i.e.*, weak (<300 °C), moderate (300–500 °C) basic sites; the desorption peak at >500 °C is attributed to the strong basic sites. The weak sites are probably the result of Brønsted basicity, which is caused by the hydroxyl groups on the surface. The medium and strong areas appear most probably related to Lewis' basicity, which arise from three and four-fold-coordinated O_2 anions, respectively. In comparison, the pristine DFNS exhibited exclusively a small desorption peak related to the region of weak basic sites. The inclusion of MgO increased the basicity of the MgO@DFNS catalyst as compared to pristine DFNS. The interaction of CO_2 with hydroxyl groups on the surface of MgO@DFNS causes desorption peaks that range between 30 and 150 °C. The desorption peaks broadening from 150 to 350 °C are due to the interaction of CO_2 to basic Mg^{2+} and O^{2-} pairs. The desorption peaks of CO_2 become more intense and larger total area in the region of weak basic sites as MgO is included in the DFNS, showing that the amount and strength of the basic sites increased with MgO loading. Similarly, Shouyun Cheng *et al.*[43] showed that adding MgO species increases the basicity of the catalyst. The CO_2 adsorption curves for MgO@DFNS showed a third peak at temperatures over 500 °C, indicating the presence of strong and isolated basic sites O^{2-}.[44] It reveals that slight basicity presents in DFNS which is calculated as 0.0328 mmol g^{-1}, however, moderated basic sites were observed in the final catalyst which is calculated as 0.152 mmol which could be favourable for the reaction to proceed.

3.2. Catalytic activity of MgO@DFNS towards the synthesis of benzimidazole derivatives

3.2.1 Effect of catalyst loading towards the synthesis of benzimidazole derivatives. After confirmation of its formation and studying its physical–chemical properties, the prepared catalysts were tested for their catalytic activity towards the synthesis of benzimidazole derivatives. In this regard, several reactions were initially conducted to optimize the catalyst loading amount, effective reaction temperature and solvent to achieve the highest conversion and yield towards benzimidazole derivatives. Firstly, we performed a reaction between OPDA (1 mmol) and aldehyde (1.2 mmol) in ethanol at room temperature for 4 h without adding a catalyst. We observed nearly only a 32% yield for the desired product (Table 2, entry 1). At the same time this reaction continued for longer time *i.e.* 16 h without catalyst and observed that 72% conversion, 54% selectivity with 60% yield (Table 2, entry 2). Hence, this reaction indicated the presence of a catalyst is important to achieve expected conversion and yield. Further, a reaction was conducted between OPDA and aldehyde with 5 wt% of catalyst and the result indicated 93% of conversion with 85% yield (Table 2, entry 3). The increase of catalyst loading to 10 wt% with the

Table 4 Synthesis of benzimidazole derivative using the different heterogeneous catalyst and their comparison with MgO@DFNS catalyst under optimized reaction conditions[a]

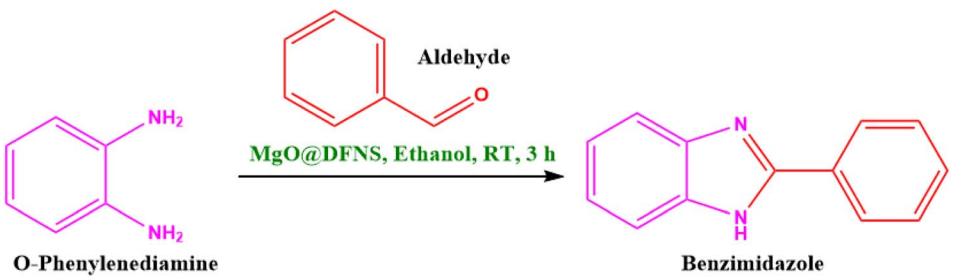

Entry	Catalyst	[b]Conv./sel. (%)	[b]Yield (%)
1	$CeCl_3 \cdot 3H_2O$	85/72	60
2	$MgCl_2$	90/71	75
3	$NiCl_2$	98/65	62
4	$CoCl_2 \cdot 7H_2O$	100/68	71
5	$Mg(NO_3)_2$	85/70	67
6	MgO	87/80	70
7	DFNS	75/55	45
8	$MgO–CeO_2@SiO_2$	92/88	85
9	**MgO@DFNS**	**100/90**	**95**
10	$CeCl_3 \cdot 3H_2O$	85/72	60

[a] Reaction conditions: all reactions proceeded with 1 mmol *o*-phenylenediamine (OPDA), 1.2 mmol aldehyde, in ethanol for 3 h. [b] Yield refers to an isolated product which characterized by ^{1}H NMR, ^{13}C NMR.

Table 5 Synthesis of different benzimidazole derivatives using MgO@DFNS catalyst under optimized reaction conditions[a]

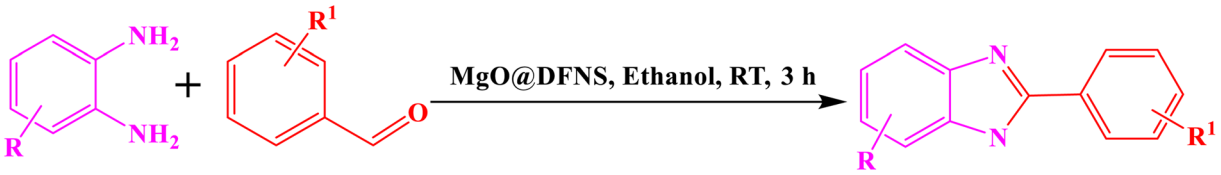

Diamine
R=Ph

Aldehyde
R^1=Cl, OCH_3, Ph, F, $COOCH_3$, Br

Benzimidazole

Entry	Reactant-1	Reactant-2	Product	Conversion (%)	[b]Yield/selectivity (%)
01	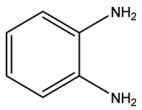	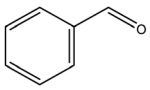	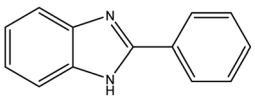	100	93/90
02	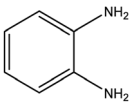	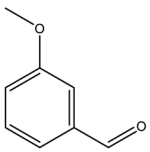	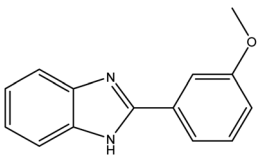	100	90/88
03	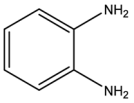	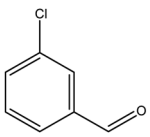	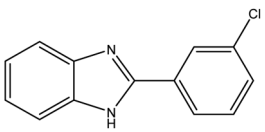	100	91/85
04	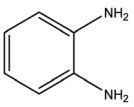	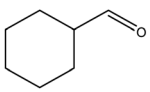	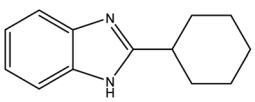	100	94/91
05	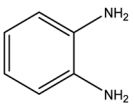	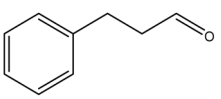	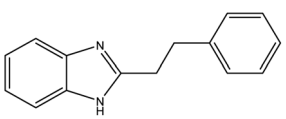	100	92/90
06	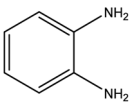	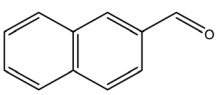	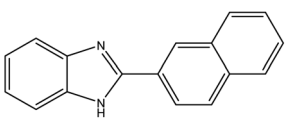	99	88/85
07	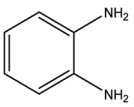	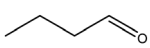	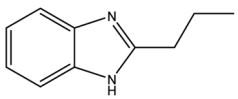	100	90/87
08	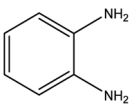	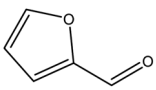	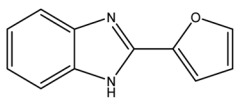	95	80/75
09	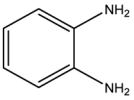	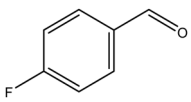	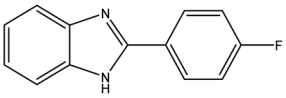	100	89/83
10	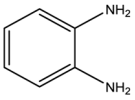	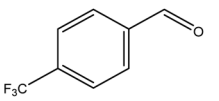	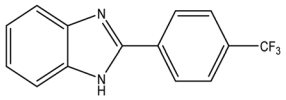	100	92/86
11	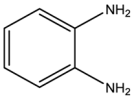	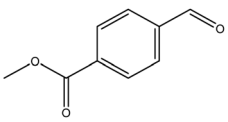	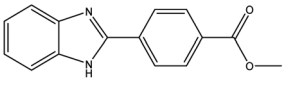	97	85/82

Table 5 (*Contd.*)

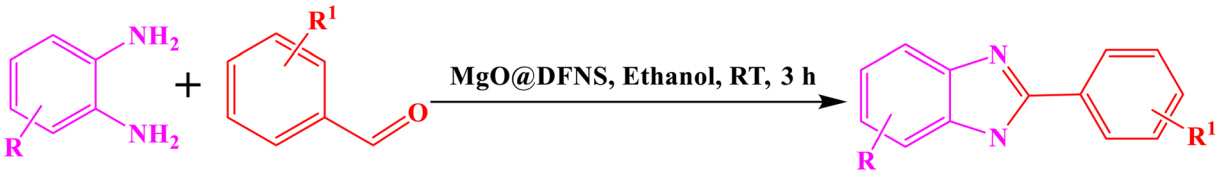

Diamine **Aldehyde** **Benzimidazole**

R=Ph **R^1=Cl, OCH_3, Ph, F, $COOCH_3$, Br**

Entry	Reactant-1	Reactant-2	Product	Conversion (%)	[b]Yield/selectivity (%)
12	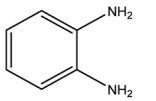	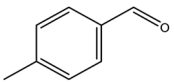	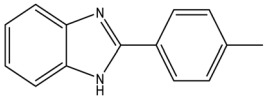	98	88/82
13	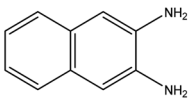	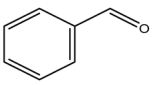	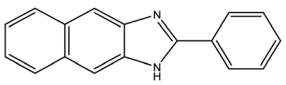	95	85/80
14	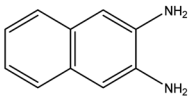	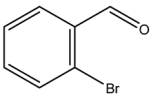	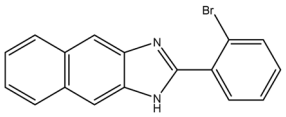	96	82/75
15	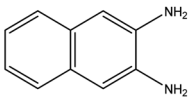	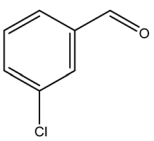	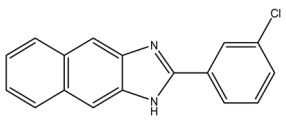	94	82/78

[a] Reaction conditions: all reactions proceeded with 1 mmol substituted *o*-phenylenediamine (OPDA), 1.2 mmol aldehyde, 5 wt% FC/AC catalyst. [b] Yield refers to isolated products which characterized by ^{1}H NMR, and ^{13}C NMR.

same reaction parameters resulted in a 100% conversion of diamine with a remarkable yield of 95% towards benzimidazole (Table 2, entry 4). After that, we increased the catalyst dosage (15 wt% and 20.0 wt%) to increase selectivity but these experiments revealed that fall in the selectivity towards the desired product (Table 2, entries 5 and 6). The decrease in selectivity occurred due to the over-reaction and formation of by-products. Hence, it is worth mentioning here that, 10 wt% of MgO@DFNS catalyst loading provided sufficient active and acidic sites for the reaction to progress in the positive direction with appreciable conversion, yield, and selectivity. Therefore, 10 wt% of MgO@DFNS catalyst loading for further reactions in this work.

3.2.2. Effect of solvents towards the synthesis of benzimidazole derivatives. The nature of the solvent also has a significant influence on the catalytic organic transformation depending on the type of catalyst employed for the reaction. Initially, we carried out a reaction without solvent resulted in 100% conversion w.r.t. diamine but the formation of byproducts was observed which leads to a loss of the selectivity (Table 3, entry 1). Hence solvent is required for this organic transformation, we have tried acetonitrile, and THF, as solvents showed 97% conversion and more than 85% selectivity (entries 2 and 3) whereas 1,4-dioxane, chloroform solvents showed similar results 85% conversion (entries 4 and 5). The polar and protic solvents such as ethanol, methanol, dimethyl formamide (DMF), ethyl acetate (entries 6–10) and also mixed solvents as a 1 : 1 ratio were also investigated (entries 11–14) and it is observed that ethanol was excellent solvent and gave good to excellent yield for the synthesis of benzimidazole among other solvents. The mixed solvents system were also fail to give efficient results as compared with the pure ethanol. Therefore, ethanol was chosen as a solvent that can be considered as an optimized condition for further applications in this manuscript.

3.3. Comparison of the present catalytic system with known catalysts for benzimidazole synthesis

To know the efficiency of the prepared MgO@DFNS catalyst towards the synthesis of benzimidazole derivatives with other known homogeneous and heterogeneous catalysts we conducted the reaction. As per the available literature, the catalysts for the synthesis of benzimidazole derivatives have different

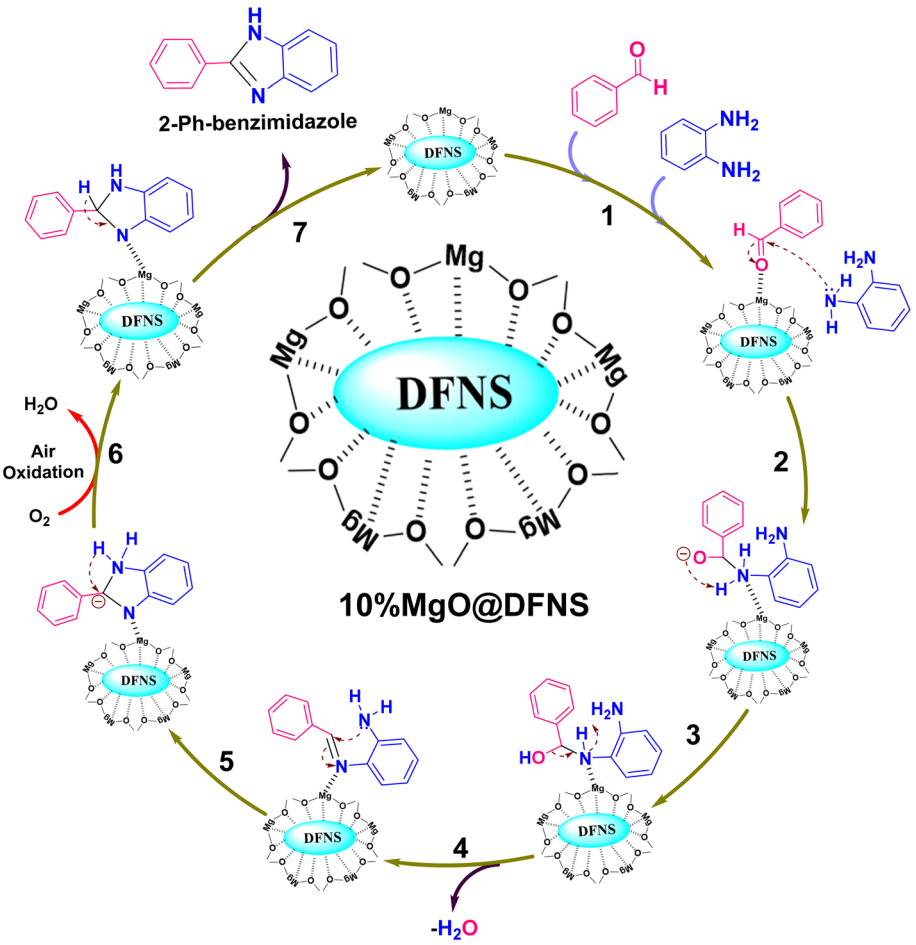

Fig. 12 Plausible reaction mechanism for 2-phenyl-benzimidazole synthesis over 10% MgO@DFNS catalyst.

reaction conditions and parameters. To compare the results and for uniformity, we have performed the same reaction under an optimized condition in the presence of different available catalysts from the literature. We have conducted the reaction with available catalysts from the literature and also with the prepared catalyst. The results are summarized in Table 4. Initially, we tried with $CeCl_3 \cdot 3H_2O$ taking optimized catalyst dosage and observed 85% conversion with moderate yield (Table 4, entry 1) subsequently we performed with $MgCl_2$, $NiCl_2$, $CoCl_2 \cdot 7H_2O$ simultaneously and observed that increasing the conversion towards di amine and also decreasing towards the selectivity (Table 4, entries 2–4). However, we have tried with $Mg(NO_3)_2$, MgO gave almost the same as earlier results, then also tried with pristine DFNS observing poor conversion concerning diamine. Finally concluded that MgO@DFNS behaved as a good selective heterogeneous catalyst under optimized conditions.

3.4. Synthesis of different benzimidazole derivatives from substituted OPDA and aldehyde by using MgO@DFNS catalyst

To investigate the catalytic activity towards benzimidazole derivatives we have explored the different reactants under optimized conditions and characterized their structures by ^1H NMR and ^{13}C NMR. The results are summarized in Table 5. In this, we have screened aromatic, aliphatic and also heterocyclic aldehydes, we studied the substrate scope with various sets of substituted aliphatic and aromatic aldehydes. It was found that all the substrates were viable in this transformation, providing benzimidazole derivatives in moderate to good yields, which has a pharmacological and biological interest.

3.5. Proposed plausible mechanism for MgO@DFNS catalyzed synthesis of benzimidazole

Fig. 12 illustrates the plausible reaction mechanism pathway for the 2-phenyl-benzimidazole product synthesis with the help of model reagents such as benzaldehyde and *o*-phenylenediamine (OPD) molecules over Lewis acidic sites containing 10% MgO@DFNS catalyst, with the support of characterization results and earlier reports.[45,46] Initially, the carbonyl group of the benzaldehyde molecule was interacted and activated with the aid of the Lewis acidic site of Mg^{2+} present the catalyst (step 1). The activated aldehyde molecule enhanced the electrophilic nature of the carbonyl carbon atom, which ultimately helps to decrease the transition state energy and attack the amino group of the OPD on the carbonyl carbon atom (step 2).[45,46] As a result of the transfer of the proton in step 3 and the elimination of the

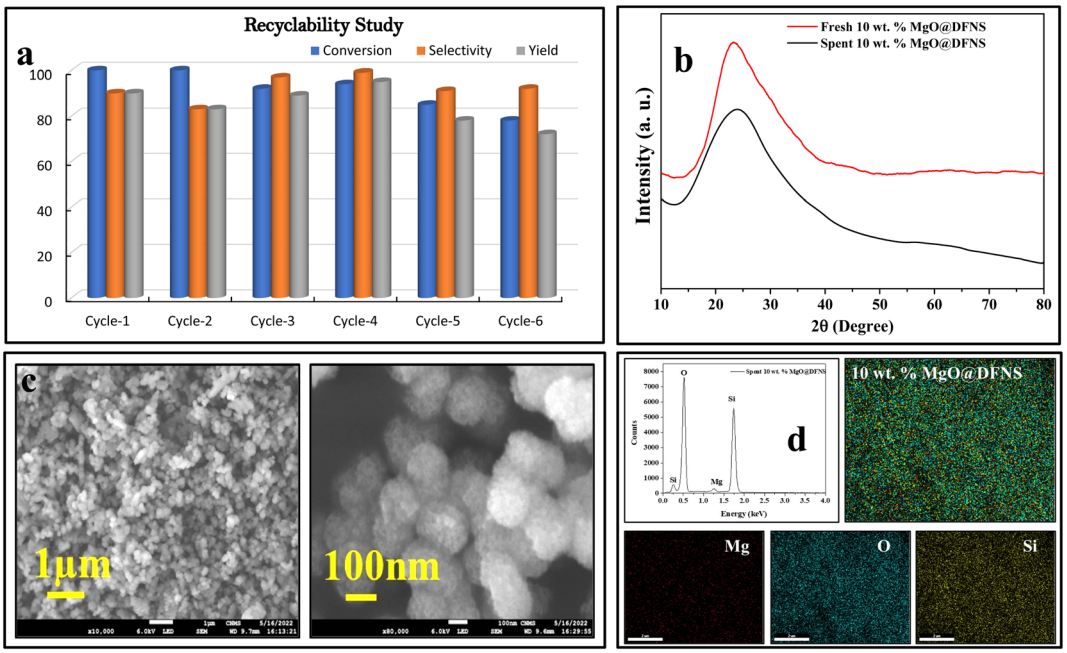

Fig. 13 Recyclability study of MgO@DFNS catalyst for the synthesis of benzimidazole product (a), XRD analysis of fresh and recycled catalyst (b), FE-SEM analysis of recycled catalyst (c) and EDX analysis and elemental mapping of recycled catalyst (d).

water molecule as side product, the stable imine (C═N) bond was formed in step 4. Furthermore, the another free amino group (NH_2) of the OPD molecule interacted with the carbon atom of the imine group. In next step, the transfer of proton was happen (step 5) and the dehydrogenation process occurred in presence of air (step 6).[47,48] Finally, the stable desired product 2-phenyl-benzimidazole was formed by the successful elimination of the catalyst surface in the reaction medium. The eradicated catalyst surface will again involve as an effective active surface to achieve the desired product in the reaction medium for the next round.

3.6. Recyclability studies

The heterogeneous catalyst is of extreme importance from an industrial viewpoint as they can be reused for a number of catalytic cycles.[21,22,24,25] To investigate the reusability performance of the present catalyst, we have performed a recyclability study of the MgO@DFNS catalyst by filtering the solid catalyst from the reaction mixture, giving an excessive amount of solvent washing several times and finally drying it under vacuum for 6 h. The dried MgO@DFNS catalyst was then used in the required amount and the reaction was performed under optimized reaction conditions. The recyclability study results are shown in Fig. 13, which revealed that the MgO@DFNS catalyst could effectively produce consistent conversion and yield towards the desired product for up to six consecutive recycles without losing noticeable activity. Additionally we have also carried our the characterisation of recycled catalyst such as XRD, FE-SEM and EDX. These recycled catalyst characterisation data revealed that, the catalyst was consistant in terms of morphology and as well as physicochemical properties up to six cycles.

4. Conclusions

In summary, we developed a mild and efficient protocol for the synthesis of benzimidazole derivatives by condensation of *o*-phenylenediamine and aldehydes using the prepared engineered MgO supported on dendritic fibrous nano-silica (MgO@DFNS) as an efficient sustainable catalyst. The prepared catalyst was thoroughly examined and characterized and it was successfully confirmed by several spectrochemical and analytical techniques such as using XRD, XPS, FT-IR, FE-SEM, HR-TEM, TPR, and NH_3-TPD analysis. The 10 wt% of MgO@DFNS catalyst was explored for its activity towards the one-pot synthesis of benzimidazole derivatives and showed remarkable results. The MgO@DFNS catalyst expressed 100% conversion and 90% selectivity and 90% yields of desired products under mild and eco-friendly reaction conditions. Furthermore, the prepared catalyst was studied for the effect of reaction parameters such as reaction time, the effect of solvents, the effect of catalyst dosage, the effect of reaction temperature, and the effect of different homogeneous and heterogeneous catalysts. To understand the substrate scope 15 different types of benzimidazole derivatives were prepared by using the different substituted diamines and substituted aldehydes under optimized reaction conditions. Additionally, the recyclability study of the catalyst was done up to 6 cycles and it was observed that, almost consistent conversion and selectivity towards desired product up to six subsequent cycles without significant loss of catalytic activity and morphology of the MgO@DFNS catalyst. Hence, the present work highlights a sustainable approach for the synthesis of benzimidazole derivatives in high yields with the help of 10 wt% MgO@DFNS as a heterogeneous catalyst under ambient temperature. We believed that these

particular findings of the new protocol may open a new green pathway for innovative synthesis of benzimidazole and its derivatives and also valuable scale-up processes of the same.

Conflicts of interest

There are no conflicts to declare.

Acknowledgements

The authors would like to acknowledge the Science and Engineering Research Board (SERB), Government of India, for financial support through Core Research Grant (CRG) file no. CRG/2021/000656.

References

1 W. A. Zoubi, *Int. J. Org Chem.*, 2013, **2013**, 73–95.
2 T. Fonseca, B. Gigante and T. L. Gilchrist, *Tetrahedron*, 2001, **57**, 1793–1799.
3 T. Roth, M. L. Morningstar, P. L. Boyer, S. H. Hughes, R. W. Buckheit and C. J. Michejda, *J. Med. Chem.*, 1997, **40**, 4199–4207.
4 M. T. Migawa, J.-L. Girardet, J. A. Walker, G. W. Koszalka, S. D. Chamberlain, J. C. Drach and L. B. Townsend, *J. Med. Chem.*, 1998, **41**, 1242–1251.
5 W. A. Denny, G. W. Rewcastle and B. C. Baguley, *J. Med. Chem.*, 1990, **33**, 814–819.
6 S. M. Sondhi, N. Singh, A. Kumar, O. Lozach and L. Meijer, *Bioorg. Med. Chem.*, 2006, **14**, 3758–3765.
7 D. Valdez-Padilla, S. Rodríguez-Morales, A. Hernández-Campos, F. Hernández-Luis, L. Yépez-Mulia, A. Tapia-Contreras and R. Castillo, *Bioorg. Med. Chem.*, 2009, **17**, 1724–1730.
8 J. D. Geratz, F. M. Stevens, K. L. Polakoski, R. F. Parrish and R. R. Tidwell, *Arch. Biochem. Biophys.*, 1979, **197**, 551–559.
9 R. W. Middleton and D. G. Wibberley, *J. Heterocycl. Chem.*, 1980, **17**, 1757–1760.
10 L. Fan, W. Chen and L. Kong, *Heterocycles*, 2015, **91**, 2306.
11 K. Bahrami, M. M. Khodaei and I. Kavianinia, *J. Chem. Res.*, 2006, **2006**, 783–784.
12 L.-H. Du and Y.-G. Wang, *Synthesis*, 2007, **2007**, 675–678.
13 M. Faheem, A. Rathaur, A. Pandey, V. Kumar Singh and A. K. Tiwari, *ChemistrySelect*, 2020, **5**(13), 3981–3994.
14 K. R. Kumar, P. V. V. Satyanarayana and B. S. Reddy, *Arch. Appl. Sci. Res.*, 2012, **4**, 1517–1521.
15 Y. Venkateswarlu, S. R. Kumar and P. Leelavathi, *Org. Med. Chem. Lett.*, 2013, **3**, 7.
16 G. R. S. Kohli, S. Hooda and R. Chandra, *Dalton Trans.*, 2021, **50**, 7750–7758.
17 A. Ben-Alloum, S. Bakkas and M. Soufiaoui, *Tetrahedron Lett.*, 1998, **39**, 4481–4484.
18 J. Lu, B. Yang and Y. Bai, *Synth. Commun.*, 2002, **32**, 3703–3709.
19 M. B. Swami, S. G. Patil, S. R. Mathapati, H. G. Ghuge and A. H. Jadhav, *Der Pharma Chem.*, 2015, **7**, 533–535.
20 M. B. Swami, A. H. Jadhav, S. R. Mathpati, H. G. Ghuge and S. G. Patil, *Res. Chem. Intermed.*, 2017, **43**, 2033–2053.
21 D. Prasad, K. N. Patil, R. B. Dateer, H. Kim, B. M. Nagaraja and A. H. Jadhav, *Chem. Eng. J.*, 2021, **405**, 126907.
22 D. Prasad, K. N. Patil, V. K. Manoorkar, R. B. Dateer, B. M. Nagaraja and A. H. Jadhav, *Mater. Manuf. Processes*, 2021, **36**, 1571–1578.
23 A. Maity, R. Belgamwar and V. Polshettiwar, *Nat. Protoc.*, 2019, **14**, 2177–2204.
24 A. H. Jadhav, A. C. Lim, G. M. Thorat, H. S. Jadhav and J. G. Seo, *RSC Adv.*, 2016, **6**, 31675–31686.
25 K. N. Patil, P. Manikanta, R. R. Nikam, P. M. Srinivasappa, A. H. Jadhav, H. P. Aytam, K. S. R. Rao and B. M. Nagaraja, *Results Eng.*, 2023, **17**, 100851.
26 A. S. Patki, K. N. Patil, S. Kusuma, D. B. Muley and A. H. Jadhav, *Res. Chem. Intermed.*, 2021, **47**, 2751–2773.
27 A. H. Jadhav, A. Chinnappan, R. H. Patil, S. V. Kostjuk and H. Kim, *Chem. Eng. J.*, 2014, **240**, 228–234.
28 J. Shabir, S. Rani, M. Sharma, C. Garkoti, Surabhi and S. Mozumdar, *RSC Adv.*, 2020, **10**, 8140–8151.
29 S. Arunmetha, A. Karthik, S. R. Srither, M. Vinoth, R. Suriyaprabha, P. Manivasakan and V. Rajendran, *RSC Adv.*, 2015, **5**, 47390–47397.
30 I. M. El-Nahhal, F. S. Kodeh, J. K. Salem, T. Hammad, S. Kuhn, R. Hempelmann and S. Al Bhaisi, *Chem. Afr.*, 2019, **2**, 267–276.
31 Z. Wang, X. Li, L. Feng, B. Liu and F. Shamsa, *Catal. Lett.*, 2021, **151**, 1911–1922.
32 M. Moradi, N. Rastakhiz, M. Ghaedi and R. Zhiani, *Catal. Lett.*, 2021, **151**, 1653–1662.
33 M. Wu, Y. Fu, W. Zhan, Y. Guo, Y. Guo, Y. Wang and G. Lu, *Catalysts*, 2017, **7**, 155.
34 X. Li, P. Xu, Y. Zhou, Y. Chen, H. Jia, H. Yu and X. Li, *Anal. Chem.*, 2022, **94**, 16502–16509.
35 A. P. Jakhade, M. V. Biware and R. C. Chikate, *ACS Omega*, 2017, **2**, 7219–7229.
36 Y. Fang, X. Wang, Q. Pan, Y. Chen and L. Dai, *Chin. Chem. Lett.*, 2021, **32**, 3976–3979.
37 X. Sun, H. T. Liu and H. F. Cheng, *RSC Adv.*, 2017, **7**, 47833–47839.
38 D. Arl, V. Roge, N. Adjeroud, B. R. Pistillo, M. Sarr, N. Bahlawane and D. Lenoble, *RSC Adv.*, 2020, **10**, 18073–18081.
39 S. E.-D. Hassan, A. Fouda, E. Saied, M. M. S. Farag, A. M. Eid, M. G. Barghoth, M. A. Awad, M. F. Hamza and M. F. Awad, *J. Fungi*, 2021, **7**, 372.
40 J. Moulder, W. Stickle, W. Sobol and K. D. Bomben, *Handbook of X-Ray Photoelectron Spectroscopy*, PerkinElmer Corporatioon, Physical Electronics Division, 1992.
41 S. Hu, Y. Zhou, C. Yuan, W. Wang, J. Hu, Q. Li and J. He, *High Volt.*, 2020, **5**, 249–255.
42 Z. Mohammadbagheri and N. Chermahini, *Renewable Energy*, 2020, **147**, 2229–2237.
43 S. Cheng, L. E. Metzger and S. I. Martinez-Monteagudo, *Sci. Rep.*, 2020, **10**, 2730.
44 L. Wang, M. Ammar, P. He, Y. Li, Y. Cao, F. Li, X. Han and H. Li, *Catal. Today*, 2017, **281**, 360–370.

45 K. Bahrami and Z. Karami, *J. Exp. Nanosci.*, 2018, **13**, 272–283.
46 A. H. Cahyana, B. Ardiansah and N. A. Asrianti, *AIP Conf. Proc.*, 2018, **2023**, 020061.
47 B. Li, R. Tayebee, E. Esmaeili, M. S. Namaghi and B. Maleki, *RSC Adv.*, 2020, **10**, 40725–40738.
48 P. L. Reddy, R. Arundhathi, M. Tripathi, P. Chauhan, N. Yan and D. S. Rawat, *ChemistrySelect*, 2017, **2**, 3889–3895.